LAWRENCE
LIVERMORE
NATIONAL
LABORATORY

LLNL-JRNL-708939

The stability of Cd1-xZnxOyS1-y quaternary alloys assessed with first-principles calculations

J. B. Varley, X. He, A. Rockett, V. Lordi

November 11, 2016

ACS Applied Materials & Interfaces

Disclaimer

LLNL-JRNL-708939

The stability of $Cd_{1-x}Zn_xO_yS_{1-y}$ quaternary alloys assessed with first-principles calculations

Joel B. Varley,*,† Xiaoqing He,‡ Angus Rockett,‡ and Vincenzo Lordi†

†*Materials Science Division, Lawrence Livermore National Laboratory, Livermore, CA 94550, USA*

‡*Department of Materials Science and Engineering, University of Illinois at Urbana-Champaign, Urbana, Illinois, 61801, USA*

Abstract: One route to decreasing the absorption in CdS buffer layers in Cu(In,Ga)Se_2 and $Cu_2ZnSn(S,Se)_4$ thin-film photovoltaics is by alloying. Here we use first-principles calculations based on hybrid functionals to assess the energetics and stability of quaternary Cd, Zn, O, and S ($Cd_{1-x}Zn_xO_yS_{1-y}$) alloys within a regular solution model. Our results identify that full miscibility of most $Cd_{1-x}Zn_xO_yS_{1-y}$ compositions and even binaries like Zn(O,S) is outside typical photovoltaic processing conditions. The results suggest that the tendency for phase separation of the oxysulfides may drive the nucleation of other phases such as sulfates that have been increasingly observed in oxygenated CdS and ZnS.

Keywords: thin-film photovoltaics, buffer layer, CIGS, CZTS, alloy, density functional theory

The attractive electronic and optical properties of binary II-VI compounds containing Cd, Zn, O, and S have made these materials staples in a number of technologies, particularly in conventional thin-film photovoltaics (PV) where they act as window and contact layers critical for high performance.[1–3] For example, in typical CdTe and Cu(In,Ga)Se_2 (CIGSe) devices, a buffer layer is incorporated between the absorber and transparent contact layers to protect the absorber while facilitating improved charge transport within the solar cell stack and often to create a *p*-*n* heterojunction. The buffer layer most often consists of chemical bath deposited (CBD) CdS due to its ease of deposition and other favorable properties such as robust *n*-type conductivity and a favorable band alignment for separation and collection of the photo-generated carriers, while (possibly doped) ZnO is the most commonly used material for the transparent contact layer.

Despite the numerous advantages of CdS as a buffer layer in thin-film PV,[1,4] it absorbs in the blue region of the solar spectrum and limits the ultimate device efficiency. The need for wider band gap buffers such as Zn(O,S,OH) has led to increasingly competitive alternatives to CdS with devices now achieving comparable efficiencies (>21% in the laboratory),[4] but these materials still represent a constrained choice for identifying optimal buffer layer compositions.

Here, we use hybrid density functional calculations to assess the stability of alloys within the quaternary space formed by Cd, Zn, O, and S to identify thermodynamically accessible compositions that may provide II-VI alternatives to CdS buffer layers. We consider the zincblende (ZB), wurtzite (WZ), and rocksalt (RS) phases spanned by the pseudobinary endpoint compounds in the $Cd_{1-x}Zn_xO_yS_{1-y}$ system, although we focus mostly on the ZB and WZ alloys that are the energetically preferred phases for dilute Zn and O concentrations and which have been observed to grow epitaxially on CIGSe absorbers using physical vapor deposition (PVD).[5]

Our calculations are based on density functional theory using the Heyd-Scuseria-Ernzerhof (HSE06) screened hybrid functional[6] and projector-augmented wave (PAW) approach[7] as implemented in the VASP code.[8] The fraction of non-local Hartree-Fock exchange (α) in the HSE functional was set to 32% to accurately reproduce the experimental band gap of CdS in the WZ phase (2.58 eV)[9–11] while simultaneously improving the calculated formation enthalpy relative to the experimental value. In Table 1 we summarize the calculated formation enthalpies of the binary II-VI reference compounds. As we focus on the energetics of the alloys, we note that the modified α improves the formation enthalpies of all compounds relative to experiment compared to a "standard" value of α=25% (see Supporting Information for more details).

We employ 64-atom ZB and RS alloy supercells based on 32-atom special quasirandom structures (SQS) for each cation and anion face-centered cubic (fcc) sublattice, which were previously generated and reported in the literature.[12] The SQS from Ref. 12 span the full composition range in increments of 6.25% for each sublattice and provide a total of $17^2 = 289$ unique stoichiometries in the ZB or RS $Cd_{1-x}Zn_xO_yS_{1-y}$ composition space. For the WZ alloys, we use 32-atom supercells based on 16-atom hexagonal-close packed (hcp) SQS also reported previously.[13] Additional details on the structures, the calculations, and the regular solution model are included in the Supporting Information.

Table 1. Summary of the calculated formation enthalpies (ΔH) used for the bulk binary references in the $Cd_{1-x}Zn_xO_yS_{1-y}$ quaternary space for different phases. The ΔH values for the ground state structures are included in bold to compare with the corresponding experimental values taken from Ref. 16.

Material	CdO	CdS	ZnO	ZnS
ΔH^{ZB} (eV)	−2.07	−1.56	−3.15	**−1.96**
ΔH^{RS} (eV)	**−2.16**	−1.32	−2.94	−1.33
ΔH^{WZ} (eV)	−2.10	**−1.57**	**−3.18**	**−1.96**
$\Delta H^{\mathrm{expt.}}$ (eV)	−2.67	−1.68	−3.64	−2.00

We note that these structures assume the randomness of the sublattices are independent, which need not be the case in alloys for more ionic compounds like the II-VI systems where clustering may be more energetically favorable. The models additionally are limited to describing the properties of solid solutions and do not account for intermixing of the sublattices or formation of other phases like sulfates and sulfites that have been observed in oxygenated CdS.[14,15] We discuss cases of competing phases later in this paper.

Within a regular solution model for heterostructural alloys, the alloy energetics can be constructed for a

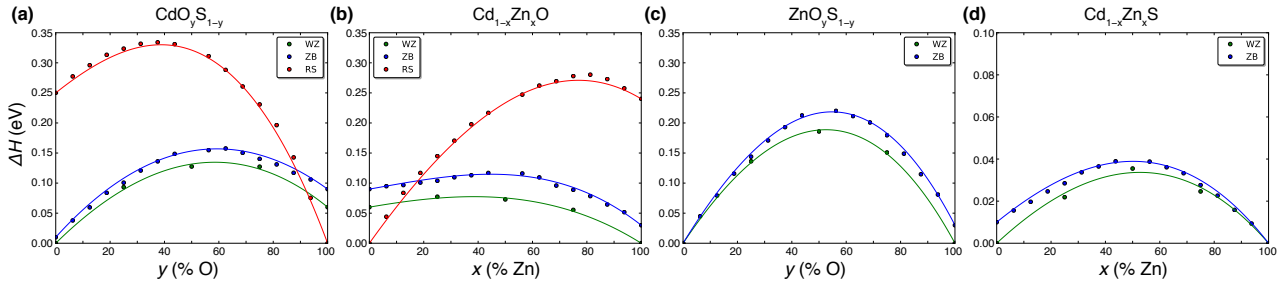

Figure 1. Plots of the mixing enthalpies for the pseudobinary II-VI alloys: CdO_yS_{1-y} (a), $Cd_{1-x}Zn_xO$ (b), ZnO_yS_{1-y} (c), and $Cd_{1-x}Zn_xS$ (d). Points are calculated using SQS, and lines show the fits to a regular solution model as described in the text and Eqn. 1. Note the difference in scale for (d).

(pseudo)binary compound

$$\Delta H(x) = x(1-x)\Omega_0 + \Omega_1(x^2-x)(x-0.5) + xE_1 + (1-x)E_0, \quad (1)$$

where Ω_0 is the regular alloy interaction parameter, Ω_1 describes the asymmetry of the enthalpy of mixing, and E_0 and E_1 are the energies of the end compounds relative to the ground state structures.[17] The mixing enthalpy describes the energy cost to form an alloy with respect to the parent compounds at zero temperature and determines whether a given alloy composition is intrinsically stable relative to phase separation. Temperature effects are included by considering the Gibbs free energy of mixing, $\Delta G(x) = \Delta H(x) - T\Delta S(x)$, with the mixing entropy $\Delta S(x)$ based on a random mixture model. Additional contributions such as the vibrational entropy are not included but not expected to influence our qualitative conclusions.

As seen from the ΔH in Table 1, the ground state structures for CdS and ZnO are the WZ phase, while CdO prefers RS and ZnS is found to be equally favorable as WZ or ZB. Figure 1 shows the computed mixing enthalpies for each of the pseudobinaries in the different phases and the excellent fits to Eqn. 1, with the obtained fit parameters included in the Supporting Information. We do not consider the RS phases for ZnO_yS_{1-y} and $Cd_{1-x}Zn_xS$ alloys due to the significantly larger formation enthalpies relative to the ZB and WZ phases in these materials (see Table 1).

The calculated mixing enthalpies are well described by Eqn. 1, with the third order Ω_1 parameter generally being largest for those containing both Zn and O. The quadratic terms Ω_0 are consistent with previous theoretical reports on the mixing enthalpies for the pseudobinary alloys.[13,17–20] Our results for the pseudobinaries identify that the Cd-containing alloys prefer the RS structure only for very high O content, above ∼87-91% O in CdO_yS_{1-y} alloys and above ∼80-86% O in $Cd_{1-x}Zn_xO$ alloys. The ranges denote the different crossover points for the WZ-RS and ZB-RS transitions, as seen in Fig. 1. For CdO_yS_{1-y} our values are in good agreement with previous theoretical reports of the transitions occurring at 84% O for the ZB to RS transition.[17] Our values for $Cd_{1-x}Zn_xO$ are also consistent with previous reports of a preference for WZ over RS alloys for Zn contents exceeding ∼5% from theoretical studies and above 31% from experiment,[21–23] and above 14% Zn for the transition to ZB from RS.[17] This suggests that alloys formed by dilute O incorporation into CdS or $Cd_{1-x}Zn_xS$ should maintain the WZ or ZB structure in the absence of phase separation.

Overall the results reveal that the energies of the WZ and ZB phases in the pseudobinary alloys are nearly equivalent for the compositions that are more S-rich, as evident from Fig. 1 in the limits of low O content. Due to the small energy differences, the preference for a given phase in practice would be more sensitive to details of the growth conditions such as the substrate orientation. This is consistent with the observed coexistence of both ZB and WZ epitaxial CdS-derived buffer layer materials in sputter-grown CIGSe thin-film photovoltaics, where the particular phase is determined by the orientation of the underlying exposed CIGSe surface facet.[5]

Most notably, we find ΔH for all the pseudobinary alloy combinations to be positive, which indicates the existence of a miscibility gap and a tendency for phase separation depending on the temperature. From our regular solution free energies, we can determine the temperatures at which the binary phases form fully miscible alloys over the entire composition range. We identify these from the common tangent construction and include the calculated binary phase diagrams in the Supporting Information. For $Cd_{1-x}Zn_xS$ WZ alloys we find miscibility starts above 210 K and all compositions become fully miscible above 800 K, the lowest of the studied alloys, while temperatures above 1140 K are necessary for the miscibility of all $Cd_{1-x}Zn_xO$ compositions. The temperatures for complete miscibility of the oxysulfides are considerably higher owing to their much larger ΔH values, with predicted temperatures of 2374 K for CdO_yS_{1-y} and 4365 K for ZnO_yS_{1-y} WZ alloys. From these thermodynamic results the oxysulfides are expected to generally suffer from significant phase separation at the microscale into regions that are highly oxygen-rich and sulfur-rich for typical PV processing conditions. This is consistent with the identification of ZnO and ZnS in X-ray absorption (XAS) spectra in Zn(O,S) thin-films grown by atomic-layer deposition (ALD) for a range of different S to O ratios.[24]

We assess the stabilities of the quaternary $Cd_{1-x}Zn_xO_yS_{1-y}$ alloys by extending the above analysis to two dimensions (see Supporting Information for more details). Considering the relatively high temperatures calculated for full miscibility of the binary alloys, we discuss specific compositions that may form stable mixtures at representative temperatures relevant to processing conditions for thin-film PV. We apply the regular solution model by defining the quaternary enthalpy of mixing using the ΔH terms fit for the pseudobinary compounds as defined by Eqn. 1 and include the results in Fig. 2(a) for heterostructural WZ alloys. The fits of the data show a mean-absolute error of 0.01 ± 0.01 eV from the

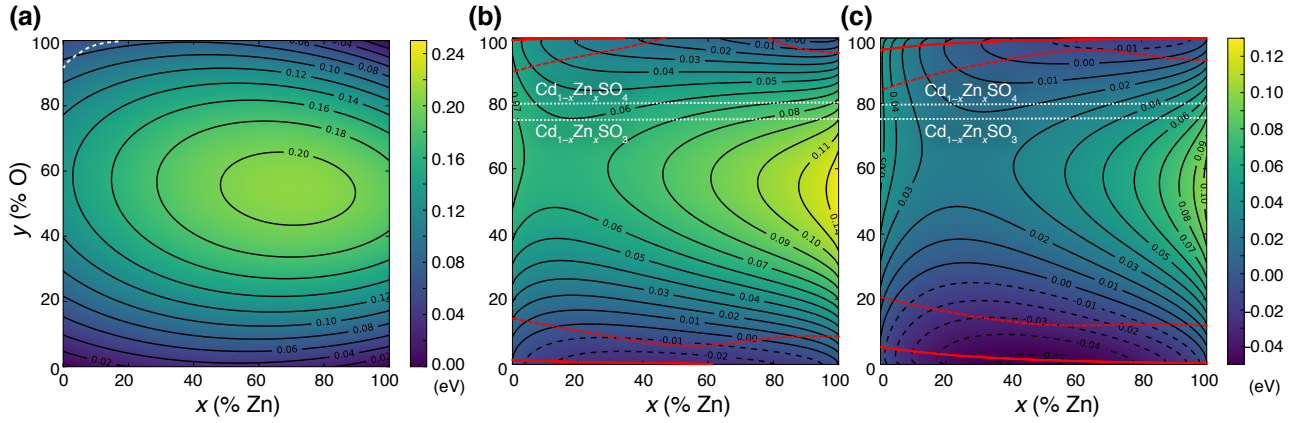

Figure 2. (a) Map of the heterostructural mixing enthalpy (ΔH) of the quaternary WZ alloys as fit within a regular solution model. The boundary denoted by the dashed white line refers to the region where RS alloys are predicted to be more favorable. The free energy of mixing (ΔG) including the entropy of random mixtures and the mixing enthalpy in (a) are included for temperatures of 1000 K (b) and 1400 K (c). The solid red lines in (b) and (c) indicate the boundaries for stable compositions while the dashed dotted red lines indicate the boundaries for spinodal decomposition. The white dotted lines denote the compositions associated with more stable sulfate and sulfite phases described in the text. The four corners in each panel represent the bulk references of CdS (lower left), CdO (upper left), ZnO (upper right), and ZnS (lower right).

ΔH explicitly calculated for the alloy structures, indicating they are well described within this two-dimensional regular solution model.

In Fig. 2 we also include results for the free energy of mixing for WZ alloys at two representative temperatures of 1000 K (b) and 1400 K (c). While these temperature ranges are above that for typical buffer-layer growth processes using CBD, they are relevant for high-temperature PVD processes. We determine the boundaries of binodal (absolute) stability regions from the conditions of equal chemical potentials of the mixtures from the common tangent construction and include these as solid red lines in Fig. 2(b) and (c). The thin regions at high and low O content above and below the red lines are stable, while the large region between them is unstable. We also compute the spinodal boundary conditions which satisfy the equations[25]

$$\left(\frac{\partial^2 G(x,y)}{\partial x^2}\right)\left(\frac{\partial^2 G(x,y)}{\partial y^2}\right) = \frac{\partial^2 G(x,y)}{\partial x \partial y}, \qquad (2)$$

where all second derivative terms are also required to be positive. The spinodal boundaries indicate where small composition fluctuations are expected to drive phase decomposition by uphill diffusion and composition waves, and are included as dashed red lines in Fig. 2(b) and (c). The regions between the binodal and spinodal boundaries are metastable, while those bounded between the dashed spinodal lines are unstable.

Inspection of the stability regions bounded by the solid red lines in Fig. 2 suggests that $Cd_{1-x}Zn_xO_yS_{1-y}$ alloys grown at typical PV processing temperatures will suffer from phase separation, as expected from the binary phase diagrams. Due to the calculated miscibility gap, quaternary solid solutions are expected only for dilute O or S concentrations (i.e. nearly $Cd_{1-x}Zn_xO$ and $Cd_{1-x}Zn_xS$) at or below the temperatures considered here. For example, we identify that at 1000 K the alloys would phase separate into low and high-O content alloys that each exhibit different phase stability. At this temperature the $Cd_{1-x}Zn_xO_yS_{1-y}$ allow full miscibility of Zn for alloys containing $\lesssim$2% O, while the O-rich compositions would additionally phase separate into solid solutions that are approximately 35% Zn and 85% Zn-content alloys owing to the immiscibility of $Cd_{1-x}Zn_xO$ alloys for all compositions at this temperature. Even at 1400 K, solid solutions are only predicted to be stable for highly O-rich and O-poor compositions ($\gtrsim$95% or $\lesssim$5% O incorporation, respectively), despite the full miscibility of the cation sublattice. This suggests that oxygenated CdS-derived materials likely exhibit a strong tendency to phase separate into highly O-rich and O-poor regions, with possible composition waves from the large spinodal decomposition region. The miscibility of the Zn-rich regions is predicted to be even lower and suggests that Zn oxysulfides are prone to phase separation at the typical temperatures involved in PV processing steps, consistent with previous theoretical investigations.[17,18,26] We note that the exact degree of phase separation may be sensitive to other details during deposition such as kinetics and even the film morphology,[27,28] so the long-term stability of Zn(O,S) and $Cd_{1-x}Zn_xO_yS_{1-y}$ alloys may require more in-depth study.

Adding to the difficulty of realizing various solid solution compositions is the possibility of the formation of competing phases with more favorable formation enthalpies than the alloy, for which we tabulate representative values in the Supporting Information. For example, we calculate the ΔH of $CdSO_4$ and $ZnSO_4$ to be -9.38 and -9.87 eV per formula unit, respectively, in their lowest energy monoclinic phases. These values are far lower than those of the parent compounds (see Table 1) and the alloys of comparable composition, which indicates a strong thermodynamic driving force for the formation of sulfates ($Cd_{1-x}Zn_xSO_4$) if sufficient O is incorporated into CdS, ZnS, or $Cd_{1-x}Zn_xS$. Other compounds such as sulfites and peroxides are also energetically favorable and likely complicate the formation of phase-pure $Cd_{1-x}Zn_xO_yS_{1-y}$ solid solutions, while the additional presence of hydrogen during growth may also facilitate the formation of hydroxide phases.[14,15,29] We include the compositions corresponding to sulfate and sulfite species in Fig. 2(b) and (c) to indicate that fall within the miscibility gap at temperatures studied. Coupled with the strong tendency for forming O-rich and O-poor $Cd_{1-x}Zn_xO_yS_{1-y}$ alloys at lower temperatures from the ΔG in Fig. 2, we believe

that the separation into O-rich regions can act as nucleation centers for these other phases that have been experimentally observed in samples prepared by a number of different deposition techniques such as sputtering,[14] atomic layer deposition,[24] and ILGAR.[30]

These competing secondary phase materials are also known to have much larger band gaps than pure CdS (>3.6 eV, see Supporting Information), and their contributions to the optical absorption and electrical transport of buffer materials remains poorly understood. For example, the calculated band gaps are 5.69 eV for $CdSO_4$, 5.32 eV for $CdSO_3$, and 3.61 eV for CdO_2, which are all far larger than the band gaps of either CdS or CdO summarized in Table 1. The properties of the film will likely depend on the precise morphology of these secondary phases, including their grain size distribution and the nature of interfaces with the host material. We still expect electron transport within the buffer to be dominated by the phases with the lowest-lying conduction bands on an absolute energy scale, which would likely be CdS or a related alloy, and this will be discussed in a future paper.

In conclusion, we report on the energetics of Zn and O mixing into CdS to form $Cd_{1-x}Zn_xO_yS_{1-y}$ quaternary alloys and identify conditions in which stable and metastable mixtures may form. We use hybrid density functional calculations to characterize the stability of ZB, WZ, and RS alloys, finding that RS quaternary alloys are only stable for alloys with very high O and Cd content, while the WZ and ZB alloys exhibit similar energies over a large region of the composition space. Either the WZ or ZB phase may be preferentially stabilized during growth depending on details of the process, such as substrate orientation. The results suggest that these alloys are prone to phase separation over a very wide composition range at typical PV processing temperatures. This instability may help drive the formation of other phases observed in oxysulfide alloys such as sulfates and sulfites that are more thermodynamically favorable and may complicate the realization of stable solid solution alloys over a wide composition range.

Supporting Information

Supporting Information with additional details of the calculations, the free energy models, and the calculated formation enthalpies and properties of sulfate and sulfite species is available free of charge via the Internet at `http://pubs.acs.org`.

Corresponding Author

*E-mail: varley2@llnl.gov

Acknowledgements

This work was performed under the auspices of the U.S. Department of Energy at Lawrence Livermore National Laboratory under Contract No. DE-AC52-07NA27344 and funded by the Department of Energy Office of Energy Efficiency and Renewable Energy (EERE) through the SunShot Bridging Research Interactions through collaborative Development Grants in Energy (BRIDGE) program.

References

(1) Naghavi, N., Abou-Ras, D.; Allsop, N.; Barreau, N.; Bücheler, S.; Ennaoui, A.; Fischer, C. H.; Guillen, C.; Hariskos, D.; Herrero, J.; Klenk, R.; Kushiya, K.; Lincot, D.; Menner, R.; Nakada, T.; Platzer-Björkman, C.; Spiering, S.; Tiwari, A. N.; and Törndahl, T. Buffer Layers and Transparent Conducting Oxides for Chalcopyrite Cu(In,Ga)(S,Se)$_2$ Based Thin Film Photovoltaics: Present Status and Current Developments. *Prog. Photovoltaics* **2010**, *18*, 411–433.

(2) Seker, F.; Meeker, K.; Kuech, T. F.; Ellis, A. B. Surface Chemistry of Prototypical Bulk II-VI and III-V Semiconductors and Implications for Chemical Sensing. *Chem. Rev.* **2000**, *100*, 2505–2536.

(3) Afzaal, M.; O'Brien, P. Recent Developments in II–VI and III–VI Semiconductors and their Applications in Solar Cells. *J. Mater. Chem.* **2006**, *16*, 1597–1602.

(4) Green, M. A.; Emery, K.; Hishikawa, Y.; Warta, W.; Dunlop, E. D. Solar Cell Efficiency Tables (Version 45). *Prog. Photovoltaics* **2015**, *23*, 1–9.

(5) He, X. Q.; Brown, G.; Demirkan, K.; Mackie, N.; Lordi, V.; Rockett, A. Microstructural and Chemical Investigation of PVD-CdS/PVD-Heterojunctions: A Transmission Electron Microscopy Study. *IEEE J. Photovoltaics* **2014**, *4*, 1625.

(6) Heyd, J.; Scuseria, G. E.; Ernzerhof, M. Hybrid Functionals Based on a Screened Coulomb Potential. *J. Chem. Phys.* **2003**, *118*, 8207.

(7) Blöchl, P. E. Projector Augmented-Wave Method. *Phys. Rev. B* **1994**, *50*, 17953–17979.

(8) Kresse, G.; Furthmüller, J. Efficiency of Ab-initio Total Energy Calculations for Metals and Semiconductors Using a Plane-wave Basis Set. *Comput. Mater. Sci.* **1996**, *6*, 15–50.

(9) Madelung, O. *Semiconductors: Data Handbook*; Springer Verlag, 2004.

(10) Varley, J. B.; Lordi, V. Intermixing at the Absorber-Buffer Layer Interface in Thin-Film Solar Cells: The Electronic Effects of Point Defects in Cu(In,Ga)(Se,S)$_2$ and $Cu_2ZnSn(Se,S)_4$ Devices. *J. Appl. Phys.* **2014**, *116*, 063505.

(11) Varley, J. B.; Lordi, V. Electrical Properties of Point Defects in CdS and ZnS. *Appl. Phys. Lett.* **2013**, *103*, 102103–102104.

(12) von Pezold, J.; Dick, A.; Friák, M.; Neugebauer, J. Generation and Performance of Special Quasirandom Structures for Studying the Elastic Properties of Random Alloys: Application to Al-Ti. *Phys. Rev. B* **2010**, *81*, 094203.

(13) Wu, J.-C.; Zheng, J.; Zacherl, C. L.; Wu, P.; Liu, Z.-K.; Xu, R. Hybrid Functionals Study of Band Bowing, Band Edges and Electronic Structures of $Cd_{1-x}Zn_xS$ Solid Solution. *J. Phys. Chem. C* **2011**, *115*, 19741–19748.

(14) Duncan, D. A.; Kephart, J. M.; Horsley, K.; Blum, M.; Mezher, M.; Weinhardt, L.; Häming, M.; Wilks, R. G.; Hofmann, T.; Yang, W.; Bär, M.; Sampath, W. S.; Heske, C. Characterization of Sulfur Bonding in CdS:O Buffer Layers for CdTe-based Thin-Film Solar Cells. *ACS Appl. Mater. Interfaces* **2015**, *7*, 16382–16386.

(15) Meysing, D. M.; Wolden, C. A.; Griffith, M. M.; Mahabaduge, H.; Pankow, J.; Reese, M. O.; Burst, J. M.; Rance, W. L.; Barnes, T. M. Properties of Reactively Sputtered Oxygenated Cadmium Sulfide (CdS:O) and their Impact on CdTe Solar Cell Performance. *J. Vac. Sci. Technol. A* **2015**, *33*, 021203.

(16) Lide, D. R. *CRC Handbook of Chemistry and Physics, 84th Edition*; CRC Handbook of Chemistry and Physics; Taylor & Francis, 2003.

(17) Lany, S. Polymorphism, Band-Structure, Band-Lineup, and Alloy Energetics of the Group II Oxides and Sulfides MgO, ZnO, CdO, MgS, ZnS, CdS. SPIE OPTO. 2014; p 89870K.

(18) Baldissera, G.; Persson, C. Understanding the Optical Properties of $ZnO_{1-x}S_x$ and $ZnO_{1-x}Se_x$ alloys. *J. Appl. Phys.* **2016**, *119*, 045704.

(19) Schleife, A.; Rödl, C.; Furthmüller, J.; Bechstedt, F. Electronic and optical properties of $Mg_xZn_{1-x}O$ and $Cd_xZn_{1-x}O$ from ab initio calculations. *New J. Phys.* **2011**, *13*, 085012.

(20) Huang, J.-D.; Liua, J.-Y.; Han, K.-L. Hybrid Functionals Studies of Structural and Electronic Properties of $Zn_xCd_{1-x}S$ and $(Zn_xCd_{1-x})(Se_xS_{1-x})$ Solid Solution Photocatalysts. *Int. J. Hydrogen Energy* **2012**, *37*, e17881.

(21) Schleife, A.; Rödl, C.; Fuchs, F.; Furthmüller, J.; Bechstedt, F. Optical and Energy-Loss Spectra of MgO, ZnO, and CdO from Ab Initio Many-Body Calculations. *Phys. Rev. B* **2009**, *80*, 035112.

(22) Schleife, A.; Eisenacher, M.; Rödl, C.; Fuchs, F.; Furthmüller, J.; Bechstedt, F. Ab Initio Description of Heterostructural Alloys: Thermodynamic and Structural Properties of $Mg_xZn_{1-x}O$ and $Cd_xZn_{1-x}O$. *Phys. Rev. B* **2010**, *81*, 245210.

(23) Detert, D. M.; Lim, S.; Tom, K.; Luce, A. V.; Anders, A.; Dubon, O. D.; Yu, K. M.; Walukiewicz, W. Crystal Structure and Properties of $Cd_xZn_{1-x}O$ Alloys Across the Full Composition Range. *Appl. Phys. Lett.* **2013**, *102*, 232103.

(24) Dadlani, A. L.; Acharya, S.; Trejo, O.; Prinz, F. B. ALD Zn(O,S) Thin Films' Interfacial Chemical and Structural Configuration Probed by XAS. *ACS Appl. Mater. Interfaces* **2016**, *8*, 14323–14327

(25) Petrishcheva, E.; Abart, R. Exsolution by Spinodal Decomposition in Multicomponent Mineral Solutions. *Acta Mater.* **2012**, *60*, 5481–5493.

(26) Janetzko, F.; Jug, K. Miscibility of Zinc Chalcogenides. *J. Phys. Chem. A* **2004**, *108*, 5449-5453.

(27) Burch, D.; Bazant, M. Z. Size-Dependent Spinodal and Miscibility Gaps for Intercalation in Nanoparticles. *Nano Lett.* **2009**, *9*, 3795–3800.
(28) Cogswell, D. A.; Bazant, M. Z. Theory of Coherent Nucleation in Phase-Separating Nanoparticles. *Nano Lett.* **2013**, *13*, 3036–3041.
(29) Mezher, M.; Garris, R.; Mansfield, L. M.; Horsley, K.; Weinhardt, L.; Duncan, D. A.; Blum, M.; Rosenberg, S. G.; Bär, M.; Ramanathan, K.; Heske, C. Electronic Structure of the Zn(O,S)/Cu(In,Ga)Se_2 Thin-Film Solar Cell Interface. *Prog. Photovoltaics* **2016**, *24*, 1142–1148.
(30) Reichardt, J.; Bär, M.; Grimm, A.; Kötschau, I.; Lauermann, I.; Sokoll, S.; Lux-Steiner, M. C.; Fischer, C. H.; Heske, C.; Weinhardt, L.; Fuchs, O.; Jung, C.; Gudat, W.; Niesen, T. P.; Karg, F. Inducing and Monitoring Photoelectrochemical Reactions at Surfaces and Buried Interfaces in Cu(In,Ga)$(S,Se)_2$ Thin-Film Solar Cells. *Appl. Phys. Lett.* **2005**, *86*, 172102.